Available online at www.sciencedirect.com

ScienceDirect

Procedia Structural Integrity 34 (2021) 51–58

Structural Integrity Procedia

www.elsevier.com/locate/procedia

The second European Conference on the Structural Integrity of Additively Manufactured Materials

The use of Additive Manufactured Inconel 625 as Bipolar Plate for the High Temperature Proton Electrolyte Membrane Fuel Cell

Jørgen Svendby[a,*], Øystein Bjelland[b], Dmitry Bokach[a], Bjarte G. B. Solheim[a]

[a]*Prototech AS, Fantoftvegen 38, NO-5072 Bergen, Norway*

[b]*Department of ICT and Natural Sciences, Norwegian University of Science and Technology (NTNU), Larsgårdsvegen 2, NO-6009 Ålesund, Norway*

Abstract

Inconel 625 is a promising candidate as base material for bipolar plates in the High Temperature Proton Electrolyte Membrane Fuel Cell (HT-PEMFC), due to its mechanical strength and anti-corrosive properties. Due to its often complicated flow channel networks both internally and externally, production time and costs are significant factors to the total fuel cell manufacturing costs. Additive manufacturing (AM) might be a promising production method, though it is important that the material have its desirable properties intact. This includes corrosion resistance towards concentrated phosphoric acid (H_3PO_4) at elevated temperatures (120 °C- 200 °C) and exposed to different voltage values. In this work, flat Inconel 625 samples have been manufactured using AM followed by post-machining of its surface to an arithmetic roughness average (R_a) of ~0.3 µm. These samples were electrochemically tested for its anti-corrosive properties while exposed to concentrated H_3PO_4 at 150 °C and a potential of 0.65 V vs the reversible hydrogen electrode (RHE). The sample surfaces were analysed using scanning electron microscopy (SEM) before and after the corrosion experiment. The interfacial contact resistance (ICR), a measure for the resistance towards electron conductivity through the corrosion-exposed surface with an adjacent conducting material, was also measured before and after the corrosion tests. For comparison, hot rolled Inconel 625 sample commercially purchased and post-machined to the same R_a-value was tested for its corrosion properties and compared to the AM-produced Inconel 625 sample. The AM-sample had a higher corrosion rate compared to the commercial with a corrosion penetration rate (CPR) almost twice as high. The measured ICR of the commercial sample was over 3.5 times higher than for the AM-sample after the corrosion test, indicating a less successful formation and thickness development of a protective phase on the AM-sample surface. Despite of equivalent surface roughness, the corrosion properties between the two production methods are significantly different, which are thought to be linked to different microstructures formed during their manufacturing.

Keywords: Additive manufacturing; Corrosion; HT-PEMFC; Bipolar Plates; Inconel 625

* Corresponding author. Tel.: +47 55 57 41 10
E-mail address: jorgen.svendby@prototech.no

10.1016/j.prostr.2021.12.008

1. Introduction

The high temperature proton exchange membrane fuel cell (HT-PEMFC) is one of many emerging fuel cell technologies believed to play a role in the future energy infrastructure. Operating in the temperature range of 120 °C-200 °C, the HT-PEMFC has numerous advantages over the more mature PEMFC-technology. Higher tolerance to inlet gas impurities, no water management, and easier cooling of the cell/stack are advantages that makes HT-PEMFC an option for systems where PEMFC cannot operate (Araya et al. (2016); Chandan et al. (2013); Rosli et al. (2017)). As with other fuel cell technologies, reducing costs, upholding the performance over time, and ensuring a sufficient lifetime of the system are the main challenges that needs to be solved.

The bipolar plates (BPPs) are among the most expensive and heaviest components in a fuel cell stack (Kundler and Hickmann (2016)). Being located between each cell, the bipolar plates have to conduct the current through the stack, provide highly optimised flow fields for the gases to ensure its homogeneous distribution over the catalyst layer, and typically have internal cooling channels for the cooling liquid necessary to control the internal stack temperature. The state-of-the-art material for HT-PEMFC is graphitic composite materials, which has to be thick due to their brittle nature, contributing to the total weight, volume, and costs of the stack (Kundler and Hickmann (2016); Weissbecker et al. (2014); Antunes et al. (2010)). Therefore, metals have been suggested as an alternative material for BPPs (Weissbecker et al. (2014)), making it possible to reduce their thickness significantly.

Another contribution to the costs is the production method. BPPs are highly complex, especially due to their intricate geometry. A possible manufacturing method that can potentially reduce costs and increase the design flexibility of the BPPs is additive manufacturing (AM). AM is well suited for making complex internal geometry that can be difficult to manufacture otherwise, especially at low production volumes. Although internal flow channels can also be achieved by laser welding of ultra-thin bipolar plates, high tooling costs prevent this manufacturing method of being profitable at low volumes. Additionally, limited dimensional stability and restricted flow channel geometry due to the manufacturing process constrain this method. In metal-AM, powder bed fusion is the most promising method for manufacturing small parts with complex geometries, and superior material quality (Pratheesh Kumar et al. (2021)). Moreover, selective laser melting (SLM) and electron beam melting (EBM) can both produce high quality metals with complex geometry. However, because the support material in the EBM process is semi-sintered during the build (Ameen et al. (2018)), extraction of powder from internal flow channels is difficult, making the EBM process less suited for manufacturing of BPPs. The SLM is not limited in extracting powder, but requires more support structures than EBM. Internal cavities, where support structures can not be removed, must therefore be designed in such a way that support structure is not necessary and unused powder can be extracted.

A challenge by using metal as material for the BPPs in HT-PEMFC is the highly corrosive environment in the cells, created by the presence of concentrated phosphoric acid (H_3PO_4) and the operational temperature and potential of the stack. In addition to potentially suffering from corrosive damage, an increase in the so-called interfacial contact resistance (ICR, the resistance towards current flow between the bipolar plate interface and the gas diffusion layer) is another potential negative effect. Due to the potentially different material structure between a traditionally produced metal and a metal produced through AM, corrosion testing of the materials and ICR-measurements are important for the validation of AM as a suitable production method for BPPs.

In this work, we present ex-situ corrosion tests of Inconel 625, a promising base material for BPP in HT-PEMFC (Nikiforov et al. (2011)). The samples tested are purchased commercially or being produced by AM in our lab, where both were machined in our workshop for equivalent surface roughness and geometry. ICR-measurements were conducted before and after. In addition, scanning electron microscopy (SEM) images before and after corrosion testing are provided.

2. Experimental

Additively manufactured Inconel 625 samples were produced in a DMG Mori Lasertec 30 selective laser melting system. The samples were additively manufactured to dimensions 5.7x42x29 mm, and were subsequently machined to final dimensions 3.7 mm x 40 mm x 27 mm and an arithmetic roughness average (R_a) of ~0.3 μm. The samples were manufactured on a stainless steel build plate with 5 mm support structure, the longest edge along the vertical axis, no build platform heating, placed diagonally along the build platform, and with a layer thickness of 50 μm. The

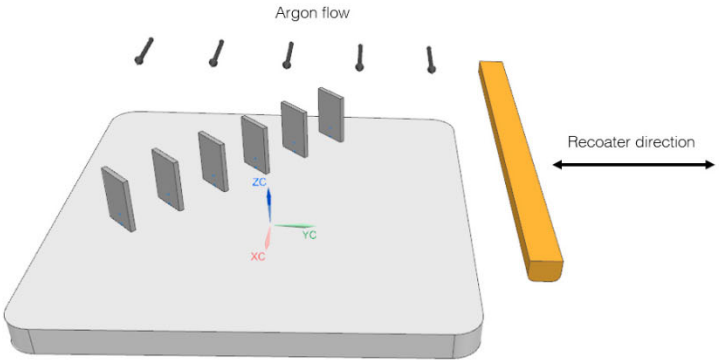

Fig. 1. Specimen build strategy.

build strategy is shown in Fig. 1, with recoater and argon flow directions indicated. For hatching, the laser speed was 0.3 m/s and the laser power 140 W, and for contouring, the laser speed was 1 m/s and power 254 W. The remaining parameters were as recommended by the manufacturer for Inconel 625. The powder was CarpenterAdditive 625 (LPW-625-AACH), batch no UK81375. The samples were not heat treated.

Reference samples of dimensions 3.7x40x27 mm were manufactured from a commercially purchased Inconel 625 hot rolled sheet (UNS N06625/ EN 2.4856). The manufacturer was VDM metals, with material certificate no. 183866/O. The original dimensions of the forged plate was 4.0x2000x6000 mm, and the heat treatment was soft annealing at 984 °C/9min/water. The commercially purchased samples were machined to a similar R_a-value and dimensions as the AM-produced samples.

The corrosion tests were conducted in a FlexCell® PTFE voltammetric cell purchased from Gaskatel, where a 3.0 cm^2 circular area of the sample surface was exposed to the electrolyte. A VMP3 potentiostat from Biologic was used to do the measurements. The cell consisted of a built-in counter electrode of a Pt/Ir-alloy, while the reference electrode was a Hydroflex® reversible hydrogen electrode (RHE) purchased from the same company. The electrolyte used for all the tests was concentrated unaltered phosphoric acid (85 % H_3PO_4 Normapur from VWR). The electrolyte was purged with N_2 for 30 minutes prior to the test, and provided above the electrolyte during the rest of the experiment to form a protective gas blanket between the atmosphere and the electrolyte. The samples were cleaned by 20 cycles of cyclic voltammetry at 100 mV/s between -0.3 V and 1.4 V vs RHE, followed by chronoamperometry at -0.5 V vs RHE for 30 seconds. The cell was heated up to 150 °C while keeping the cell at open-circuit potential (OCP). At 150 °C, a linear sweep at 1.0 mV/s from -0.3 V to maximum 1.4 V vs RHE was conducted. Finally, chronoamperometry at 0.65 V vs RHE was conducted for 24 hours, this to recreate the potential a HT-PEMFC cathode experience during normal operation (Kaserer et al. (2013); Li et al. (2018)).

The interfacial contact resistance (ICR) was measured ex-situ before and after the corrosion experiments. The principles of the measurements and subsequent calculations to obtain the ICR-values have been described in numerous publications (Avasarala and Haldar (2009); Chanda et al. (2018); Gabreab et al. (2014); Wang et al. (2003)). The sample was sandwiched between two Elat Hydrophilic plain cloths (Elat-H), which was then placed between two gold-coated copper cylinders, providing a compression pressure. The compression was measured by a load cell (Burster, 8532-5500-V400). A current of 1.0 A was provided by a Aim-TTi Digital Power Supply and the potential was measured by a 7562 Multimeter from Yokogawa. To eliminate the measurement between the carbon cloth and the gold-coated copper, a measurement of a sandwiched carbon cloth was performed separately.

Scanning electron microscopy (SEM) surface analysis of the samples were conducted by a ZEISS SUPRA 55VP instrument before and after the corrosion experiments.

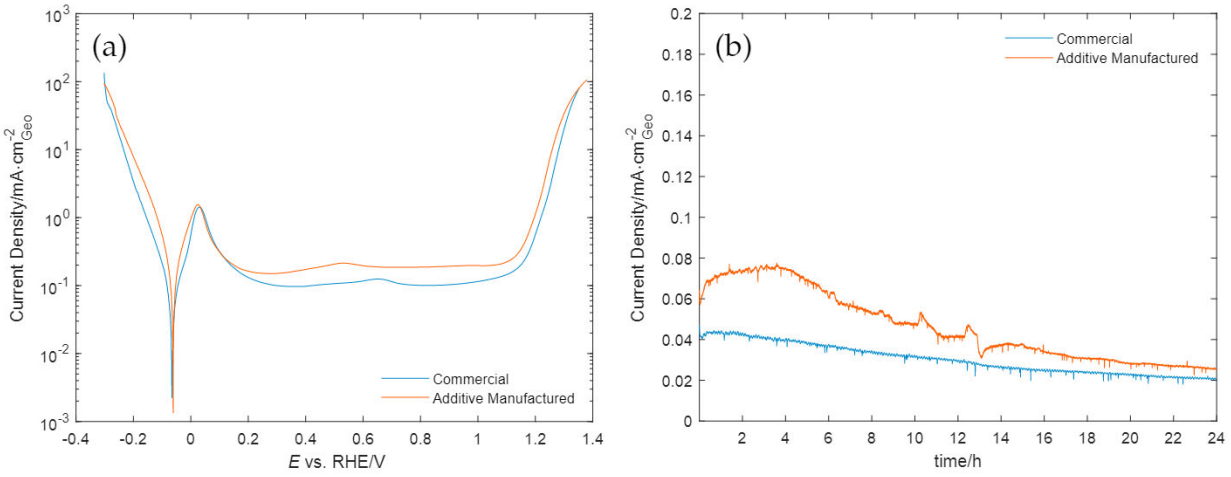

Fig. 2. (a) Linear sweep voltammetry from -0.3 V to ~1.4 V vs RHE at a sweep rate of 1.0 mV/s for the commercial and the additive manufactured Inconel 625 samples in 85 % H_3PO_4 at 150 °C. (b) Chronoamperometry (constant potential) at 0.65 V vs RHE for 24 hours in 85 % H_3PO_4 at 150 °C for the commercial and the AM-sample. The current is normalised with the geometrical area (3.0 cm^2) of the sample exposed to the electrolyte for both plots.

3. Results

Fig. 2 (a) shows the linear sweep from -0.3 V to ~1.4 V vs RHE at 1.0 mV/s of one of the tested commercial and additive manufactured Inconel 625 samples in 85 % H_3PO_4 at 150 °C. At the potential range from -0.3 V to the dip (located at -65.9 mV for the commercial sample and -61.5 mV for the AM-sample) reduction reaction takes place. At the mentioned dip, known as the corrosion potential (E_{corr}), the reduction and oxidation (corrosion) reactions are in equilibrium. At more positive potentials, a net corrosion reaction takes place. A peak at 28 mV vs RHE can be observed. This is reported in the corrosion literature as the formation of a precipitate phase, normally being an oxide (Stansbury and Buchanan (2000)). This phase partially protects the sample, keeping the current density (which is directly linked to the corrosion rate) close to constant from 0.2 V up to 1.1 V. Tiny peaks can be observed at 0.65 V for the commercial sample, and 0.52 V for the AM-sample. These peaks are probably caused by oxidation of a different species in the samples. Close to 1.1 V, the current density starts to rapidly increase with increasing potential. This is believed to be where the protective phase disappears, increasing the corrosion rate significantly (Stansbury and Buchanan (2000)).

Fig. 2 (b) shows the chronoamperometry measurement at 0.65 V vs RHE for 24 hours in 85 % H_3PO_4 at 150 °C. As reported in the literature, the cathode of a HT-PEMFC during normal steady-state operational conditions will experience a potential of 0.65 vs RHE (Kaserer et al. (2013); Li et al. (2018)). As can be seen, the current density is higher in the beginning followed by a steady decrease with time. This is due to the thickness increase of the protective phase, reducing the corrosion process of the samples with time. During the whole test, the AM-sample has a larger current, indicating a larger corrosion rate. For both samples, the current density increases in the beginning, with a larger and prolonged increase for the AM-sample. For the AM-sample, there are some prolonged fluctuations in the time interval 10 - 14 hours. The exact reason for this is unknown.

Table 1 lists the corrosion potentials (E_{corr}), corrosion current densities (j_{corr}), and the corrosion penetration rates (CPR) of the commercial- and the AM-sample. E_{corr} is obtained by the global minimum current density of Fig. 2 (a). The corrosion current density (j_{corr}) can be obtained by extrapolation of the Tafel-slopes from the oxidation- and reduction-half cell reactions, also obtained from Fig. 2 (a) (Stansbury and Buchanan (2000)). CPR can be calculated from j_{corr} by equation 1:

Table 1. Corrosion potential (E_{corr}), corrosion current density (j_{corr}), and corrosion penetration rates (CPR) for the commercial and the additive manufactured sample in 85 % H_3PO_4 at 150 °C.

	Commercial	Additive Manufactured
E_{corr}/mV	-65.9	-61.5
j_{corr}/μA/cm^2	160	300
CPR/mm/yr	0.94 - 2.7237	1.7615 - 5.0896

$$CPR = \frac{K \cdot EW \cdot j_{corr}}{\rho} \tag{1}$$

where ρ is the material density (8.44 g/cm^3), K is a constant equal to 3.27×10^{-3} mm $\cdot$ g/μA $\cdot$ cm $\cdot$ yr, and EW is given by:

$$EW = \frac{100}{\sum_{i=1}^{n} \frac{\text{wt}\%_i \cdot n_i}{M_i}} \tag{2}$$

where wt%$_i$ is the weight percent given from the material certificate, n_i is the valence number, and M_i is the the molar mass (g/mol) for the ith element of the alloy. Since the valence numbers for the elements are not known, their maximum and minimum valence numbers were used to calculate CPR, giving a CPR-range for the samples. As seen in the table, E_{corr} for the two samples are almost identical, which could be expected due to their similar elemental composition. In contrast, the j_{corr} and CPR are significantly larger for the AM-sample.

Fig. 3 shows the measured ICR-values for the commercial- and AM-sample before and after the corrosion test with a constant current of 1.0 A and at a compression value of 140 N/cm^2, which is the normal compression force for a fuel cell stack. As seen, the ICR-value is higher after the corrosion test, believed to be caused by the lower current conductivity of the protective phase formed during corrosion. The increase is especially large for the commercial sample, with an increase close to 20 times the original value, while for the AM-sample the increase is close to 2.5 times the original value.

Fig. 4 shows SEM-images of the commercial- and AM-sample surfaces before and after the corrosion tests. The images before the corrosion shows smooth surfaces with only small imperfections for both samples. The images of the samples after the corrosion tests clearly shows numerous small holes in their surface, a phenomena known as pitting corrosion. This occurs due to local non-uniform corrosion of the sample surface, which can be caused by structural imperfections (grain boundaries, scratches, dislocations etc.) and non-uniform phase- and elemental distribution in the surface. Another observation, despite being more qualitative, is the higher frequency of pits in the AM-sample surface.

4. Discussion

As is evident from Fig. 2 is the higher corrosion rate of the AM-sample compared to the hot rolled sheet commercial sample. This is also reflected by the close-to-double value of corrosion current and consequently CPR shown in Table 1. This observation can have a connection to the ICR-measurements depicted in Fig. 3. The significantly larger value after the corrosion test for the commercial sample compared to the AM-sample suggests a formation of a more stable and potentially thicker protective phase, inhibiting the corrosion reaction. Microstructural characterisation of AM

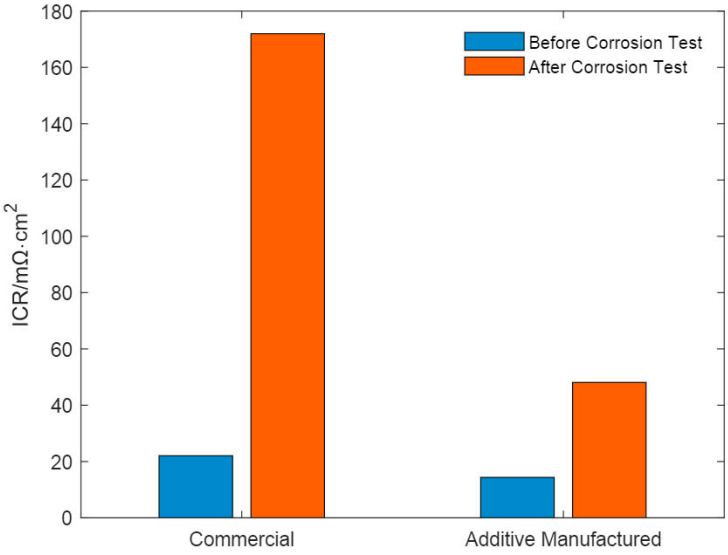

Fig. 3. ICR-measurement at a compression value of 140 N/cm^2 and a constant current of 1.0 A of the commercial and additive manufactured sample before and after the corrosion test.

nickel superalloys reported in the literature is consistent on a higher degree of imperfections in the material structure compared to traditionally produced materials (Sanchez et al. (2021); Li et al. (2015); Nguejio et al. (2019)). The main reason is the high temperature gradient formed during manufacturing, which creates an anisotropic structure particularly in the build direction. Columnar dendrites with mostly the alignment < 001 > from the sample substrate towards the building direction have been reported for Inconel 625 (Li et al. (2015); Nguejio et al. (2019)). In addition, formation of pores, cracks, and melt pool boundaries frequently happens, which can potentially be sites promoting corrosion (Kong et al. (2019)). As witnessed from Fig. 4, it is clear from the corrosion pitting formation that there are more sites prone to corrosion available on the AM-sample compared to the commercial hot rolled sample, despite of the similar roughness of the surface through machining. It is therefore clear that the complicated microstructure of the AM-sample affects the corrosion properties of the material independent of roughness factor.

This study has not included post processing strategies such as heat treatment or post hot isostatic pressing (HIP) for the AM sample. Post-HIP has been pointed out as a promising method for reducing porosity and internal defects in AM-parts. However, (Kreitcberg et al. (2017)) found that post-HIP reduced the material anisotropy for SLM Inconel 625, but at the expense of grain size. Moreover, (Ameen et al. (2018)) found that corrosion resistance of SLM 316 was worsened after post-HIP. These effects should be further explored. Likewise should effects on corrosion properties from build strategies minimising temperature gradients, such as part orientation, hatching patterns, and bed/chamber heating, also be investigated. An understanding of how to manipulate the material microstructure and its effects on the material corrosion properties are thus necessary for successfully utilising AM as a method to manufacture BPPs for HT-PEM fuel cells.

5. Conclusion

Commercial hot-rolled samples and additive manufactured samples post-machined to the same R_a-value were corrosion tested in a HT-PEMFC simulated environment (85 % H_3PO_4-electrolyte at 150 °C), where both ICR-measurements and SEM-analysis of the samples were conducted before and after the corrosion experiments. The corrosion rate of the AM-samples were significantly larger, in addition to a lower ICR-value, indicating a lower affinity to create a stable and thick enough protective phase, despite having the same R_a-value. It is clear that the formation of such a phase and the corrosion rate are linked to the microstructure of the samples, created during their manufacturing. Extensive work to understand how to achieve a desired microstructure during manufacturing, and its effect on cor-

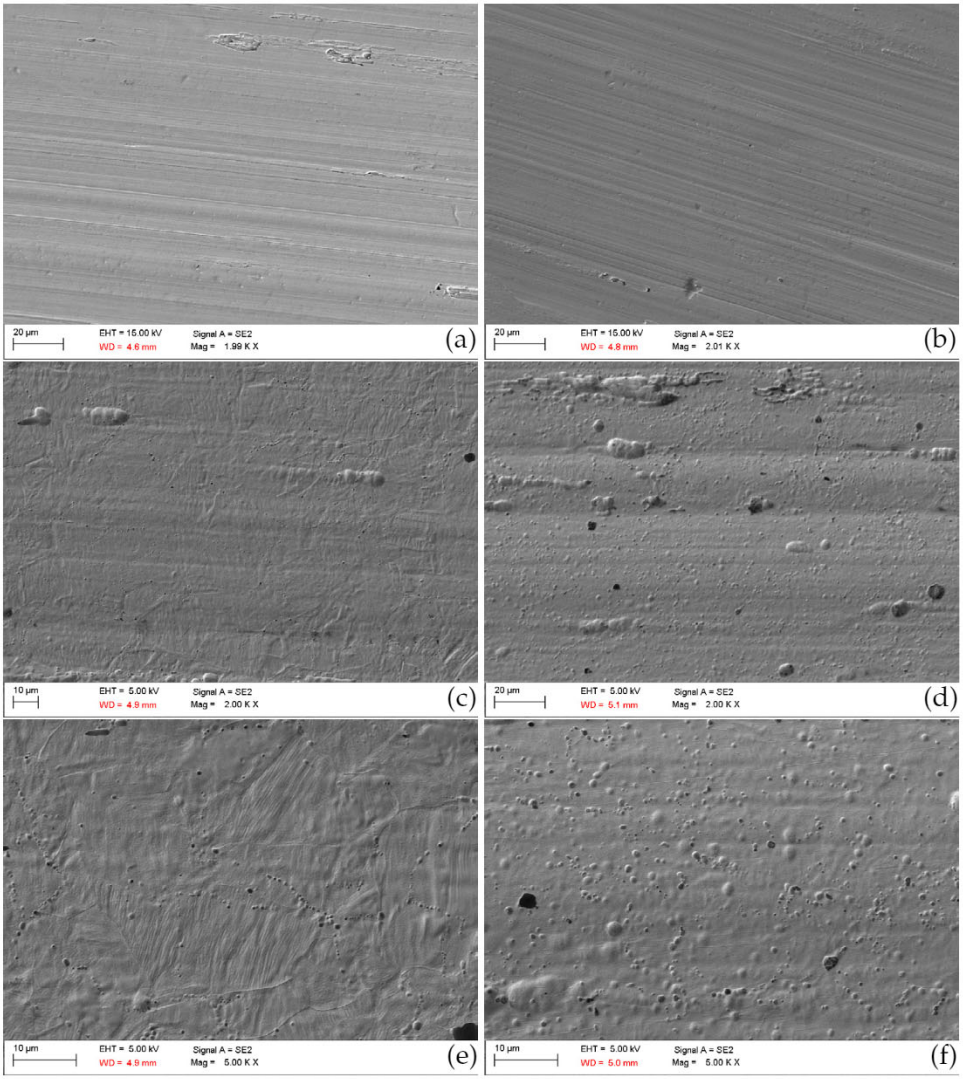

Fig. 4. SEM-images of (a) the commercial sample before corrosion test, (b) the AM-sample before the corrosion test, (c) and (e) the commercial sample after corrosion test, (d) and (f) AM-sample after the corrosion test.

rosion and protective phase formations are therefore needed to successfully implement AM as a BPP-manufacturing technique.

Acknowledgements

The works presented in this paper was performed under programme of and funded by the European Space Agency (ESA Contract No. 4000126860). The view expressed herein can in no way be taken to reflect the official opinion of the European Space Agency.

References

Ameen, W., Al-Ahmari, A., Mohammed, M.K., Mian, S.H., 2018. Manufacturability of Overhanging Holes Using Electron Beam Melting. Metals 8, 397. URL: https://www.mdpi.com/2075-4701/8/6/397, doi:10.3390/met8060397. number: 6 Publisher: Multidisciplinary Digital Publishing Institute.

Antunes, R.A., Oliverira, M.C.L., Ett, G., Ett, V., 2010. Corrosion of Metal Bipolar Plates for PEM Fuel Cells: A Review. Int. J. Hydrogen Energ 35, 3632–3647. doi:10.1016/j.ijhydene.2010.01.059.

Araya, S.S., Zhou, F., Liso, V., Sahlin, S.L., Vang, J.R., Thomas, S., Gao, X., Jeppesen, C., Kær, S.K., 2016. A Comprehensive Review of PBI-Based High Temperature PEM Fuel Cells. Int. J. Hydrogen Energ 41, 21310–21344. doi:10.1016/j.ijhydene.2016.09.024.

Avasarala, B., Haldar, P., 2009. Effect of Surface Roughness of Composite Bipolar Plates on the Contact Resistance of a Proton Exchange Membrane Fuel Cell. J. Power Sources 188, 225–229. doi:10.1016/j.jpowsour.2008.11.063.

Chanda, U.K., Behera, A., Roy, S., Pati, S., 2018. Evalutaion of Ni-Cr-P Coatings Electrodeposited on Low Carbon Steel Bipolar Plates for Polymer Electrolyte Membrane Fuel Cell. Int. J. Hydrogen Energ 43, 23430–23440. doi:10.1016/j.ijhydene.2018.10.218.

Chandan, A., Hattenberger, M., El-kharouf, A., Du, S., Dhir, A., Self, V., Pollet, B.G., Ingram, A., Bujalski, W., 2013. High Temperature (HT) Polymer Electrolyte Membrane Fuel Cells (PEMFC) - A Review. J. Power Sources 231, 264–278. doi:10.1016/j.jpowsour.2012.11.126.

Gabreab, E.M., Hinds, G., Fearn, S., Hodgson, D., Millichamp, J., Shearing, P.R., Brett, D.J.L., 2014. An electrochemical Treatment to Improve Corrosion and Contact Resistance of Stainless Steel Bipolar Plates used in Polymer Electrolyte Fuel Cells. J. Power Sources 245, 1014–1026. doi:10.1016/j.jpowsour.2013.07.041.

Kaserer, S., Rakousky, C., Melke, J., Roth, C., 2013. Design of a Reference Electrode for High-Temperature PEM Fuel Cells. J. Appl. Electrochem. 43, 1069–1078. doi:10.1007/s10800-013-0567-9.

Kong, D., Dong, C., Ni, X., Li, X., 2019. Corrosion of Metallic Materials Fabricated by Selective Laser Melting. npj Mater. Degrad. 3. doi:10.1038/s41529-019-0086-1.

Kreitcberg, A., Brailovski, V., Turenne, S., 2017. Effect of heat treatment and hot isostatic pressing on the microstructure and mechanical properties of Inconel 625 alloy processed by laser powder bed fusion. Materials Science and Engineering: A 689, 1–10. URL: https://www.sciencedirect.com/science/article/pii/S0921509317301946, doi:10.1016/j.msea.2017.02.038.

Kundler, I., Hickmann, T., 2016. Bipolar Plates and Gaskets: Different Materials and Processing Methods, in: Li, Q., Aili, D., Hjuler, H.A., Jensen, J.O. (Eds.), High Temperature Polymer Electrolyte Membrane Fuel Cells - Approaches, Status, and Perspectives. Springer International Publishing, Switzerland. chapter 19, pp. 425 – 440. doi:10.1007/978-3-319-17082-4.

Li, R., Cai, Y., Wippermann, K., Lehnert, W., 2018. Corrosion and Electrical Properties of SS316L Materials in the Simulated HT-PEFC Environment. J. Electrochem. Soc. 165, C681–C688. doi:10.1149/2.1221810jes.

Li, S., Wei, Q., Shi, Y., Zhu, Z., Zhang, D., 2015. Microstructure Characteristics of Inconel 625 Superalloy Manufactured by Selective Laser Melting. J. Mater. Sci. Tech. 31, 946–952. doi:10.1016/j.jmst.2014.09.020.

Nguejio, J., Szmytka, F., Hallais, S., Tanguy, A., Nardone, S., Martinez, M.G., 2019. Comparison of Microstructure Features and Mechanical Properties for Additive Manufactured and Wrought Nickel Alloys 625. Mater. Sci. Eng. A 764, 138214–138225. doi:10.1016/j.msea.2019.138214.

Nikiforov, A.V., Petrushina, I.M., Christensen, E., Tomás/García, A.L., Bjerrum, N.J., 2011. Corrosion Behaviour of Construction Materials for High Temperature Steam Electrolysers. Int. J. Hydrogen Energ 36, 111–119. doi:10.1016/j.ijhydene.2010.09.023.

Pratheesh Kumar, S., Elangovan, S., Mohanraj, R., Ramakrishna, J., 2021. Review on the evolution and technology of State-of-the-Art metal additive manufacturing processes. Materials Today: Proceedings , S2214785321017120URL: https://linkinghub.elsevier.com/retrieve/pii/S2214785321017120, doi:10.1016/j.matpr.2021.02.567.

Rosli, R.E., Sulong, A.B., Daud, W.R.W., Zulkifley, M.A., Husaini, T., Rosli, M.I., Majlan, E.H., Haque, M.A., 2017. A Review of High-Temperature Proton Exchange Membrane Fuel Cell (HT-PEMFC System. Int. J. Hydrogen Energ 42, 9293–9314. doi:10.1016/j.ijhydene.2016.06.211.

Sanchez, S., Smith, P., Xu, Z., Gaspard, G., Hyde, C.J., Wits, W.W., Ashcroft, I.A., Chen, H., Clare, A.T., 2021. Powder Bed Fusion of Nickel-Based Superalloys: A Review. Int. J. Mach. Tools Manuf. 165. doi:10.1016/j.ijmachtools.2021.103729.

Stansbury, E.E., Buchanan, R.A., 2000. Fundamentals of Electrochemical Corrosion. ASM International, Materials Park, Ohio.

Wang, H., Swekart, M.A., Turner, J.A., 2003. Stainless Steel as Bipolar Plate Material for Polymer Electrolyte Membrane Fuel Cells. J. Power Sources 115, 243–251. doi:10.1016/S0378-7753(03)00023-5.

Weissbecker, V., Wippermann, K., Lehnert, W., 2014. Electrochemical Corrosion Study of Metallic Materials in Phosphoric Acid as Bipolar Plates for HT-PEFCs. J. Electrochem. Soc. 161, F1437–F1447. doi:10.1149/2.0691414jes.